Presented at the 9th International
Congress on Electron Microscopy,
Toronto, Canada, August 1-9, 1978

LBL-7677

ADVANCES IN CHARACTERIZATION OF MATERIALS: ALLOYS AND CERAMICS

Gareth Thomas

May 1978

Prepared for the U. S. Department of Energy
under Contract W-7405-ENG-48

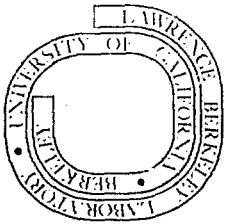

LBL-7677

ADVANCES IN CHARACTERIZATION OF MATERIALS: ALLOYS AND CERAMICS

Gareth Thomas

Department of Materials Science and Mineral Engineering, College of Engineering, and Materials and Molecular Research Division, Lawrence Berkeley Laboratory, University of California, Berkeley, California 94720

1. Introduction

The properties of materials are structure-sensitive. Structure is in turn determined by composition, heat-treatment and processing. Thus it is necessary to characterize both composition and microstructure at the highest levels of resolution possible in order to understand materials behavior. Such characterization requires advanced and sophisticated methods of analysis using microscopic, diffraction and spectroscopic techniques. For this of course electron microscopy is particularly versatile, since we are now routinely synthesizing structure almost at atomic levels of resolution. The interaction between composition, heat treatment and properties is complex but this interaction must be understood if materials are to be improved or new materials to be designed.

Figure 1 shows a schematic indicating the important role that electron microscopy now plays in research in materials science and engineering (e.g., failure analysis). The problem solving approach is not limited to a single technique and it is not implied that electron microscopy can solve all problems but clearly the method is very powerful. For certain applications high voltage microscopy shows a great expansion in the type of materials that can be studied[1] due to its advantages[2] with regard to ionisation damage and improved resolution both in imaging and diffraction). For all applications composition analysis by spectroscopy[3] and high resolution lattice parameter measurements[4] is essential. The new analytical instruments with microdiffraction and X-ray and electron energy loss microanalytical capabilities are welcome additions to the materials scientists "bag of tools" as these methods offer large gains in spatial resolution compared to more conventional analytical methods.

In this review I will draw on examples from some of the current research programs going on in my group, with particular emphasis on high resolution methods, including lattice imaging and microanalysis. For close-packed structures as is common in metals and alloys and many ceramics, point resolutions better than about 2Å are needed for structure imaging and with present day instruments this is not yet possible. This we are limited to lattice imaging for HREM studies of these materials. The researchers involved are acknowledged at the appropriate places in this paper and I express my gratitude to them for their assistance.

2. Metallic Alloys

A. Morphology, Crystallography and Formation of Dislocated Lath Martensites in Steels. (B. V. N. Rao)

Although the morphology and crystallography of plate martensites are well understood, the same is not true for the dislocated "lath" martensite occuring in the technologically more important medium and low C steels. A detailed electron diffraction and microscopy examination of dislocated lath martensites has been undertaken partly stimulated by the detection through careful dark-field analysis of small amounts of retained austenite in many lath martensites during an extensive alloy design program on dislocated martensitic steels[1]. Consequently, the unique orientation relationships can be obtained directly by utilizing selected area diffraction analysis of the lath bundles and the surrounding austenite[2]. The present discussion will be limited to results on binary Fe-Ni alloys (Table I).

Table I

Chemistry of the alloys and their M_s structures

Alloy #	Alloy Comp. (wt%), Nomial	M_s (°C)
1)	Fe-12 Ni	300*
2)	Fe-15 Ni	250*
3)	Fe-20 Ni	165*

*calculated

Morphology and Cell Structure of Martensite

The martensite packet size was found by optical microscopy to increase with austenitizing temperature and prior austenite grain size, although there was no similar variation in the average lath width. Therefore, the aspect ratio of the laths increases with prior austenite grain size. A constant aspect ratio with increasing packet size would result in a higher volume dependent strain energy. Transmission electron micrographs taken at 100 kV and 500 kV (Fig. 2(a)) revealed that the laths are parallel with reasonably straight boundaries and a high dislocation density. Although there were no significant differences in lath morphology or substructure as a function of carbon content, retained austenite could only be detected in carbon containing alloys. The advantages of using 500 kV are in the increased accuracy of selected area diffraction for the analyses described below. Knock-on damage is negligible at this voltage.

Relative Orientation of Adjacent Laths

Figure 2 is an example of the detailed analysis of parallel "laths" in the packet martensite. The SAD patterns (Fig. 2(b)) and regions from where the patterns were obtained in the bright field image (Fig. 2(a)) are identified by 1, 2, 3. The [110]$_\alpha$ crystal direction remains parallel in all the laths in this packet indicating that these laths are separated by [110] rotation boundaries. Fig. 3 shows a typical stereographic analysis of relative orientations of adjacent laths of a packet in these binary Fe-Ni alloys. From Fig. 3, it was found that lath 5 is rotated 180° with respect to lath 1 indicating that the shear components are opposite and accommodative. The present observations suggest that the orientation of the laths in a given packet are those that result from minimization of the overall shape deformation and its accommodation over a group of laths. Our work also shows that a gradual change in orientation to minimize shape deformation is preferred to a twin orientation of the adjacent laths, although the tendency for the latter increases with carbon content. It is suggested that the austenite-martensite interface may be a ledge boundary and that the macroscopic and microscopic habit planes could be different[3]. It is also concluded that the martensite laths are indeed thin platelets and that individual laths and not the packets are the fundamental nucleation events.

In order to prove these suggestions lattice imaging techniques are being utilized to analyse the austenite-martensite interfaces. These experiments are extremely

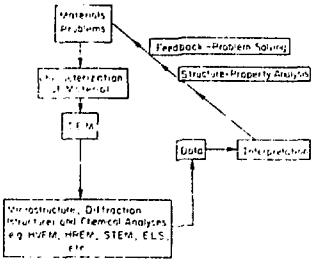

XBL 785-5018

FIG. 1

FIG. 1

Schematic showing role of electron microscopy in materials research.

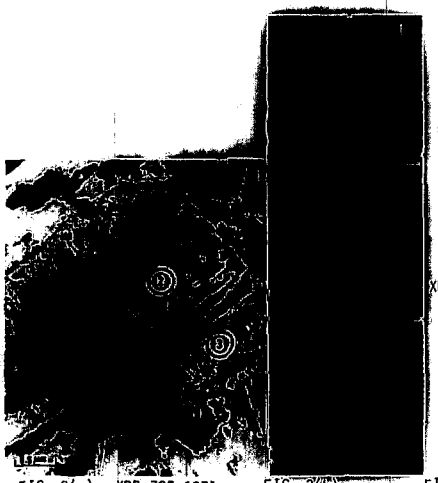

FIG. 2(a) XBB 785 6071

500 kV Bright field images of a packet of dislocated martensite in Fe-15%Ni.

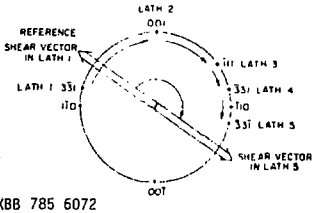

XBB 785 6072

FIG. 2(b)

Selected area diffraction patterns from the laths indicated in the packet of Fig. 2(a).

LATH REGION		ROTATION (DEGREES)
FROM	TO	
1	2	76.75
2	3	54.71
3	4	22.01
4	5	26.53
		180 TOTAL

XBL 7710 6265

FIG. 3

FIG. 3

Typical stereographic projection of orientation amongst laths in a packet of binary Fe-Ni alloys; notice rotation of adjacent laths.

difficult due to the astigmatism corrections (martensite is magnetic, austenite is not). Measurements of fringe spacings in 101 planes also enable carbon contents to be estimated. Such analysis is not possible by X-ray STEM microanalysis.

B. Grain Boundaries and Grain Boundary Precipitation (Al-Zn Alloys), (R. Gronsky)

The ability to detect highly localized compositional variations is a very desirable characteristic for experimental studies of grain boundaries. In current analysis of grain boundary precipitation reactions[7] we have used lattice imaging, from which fringe spacing measurements have given clear indications of composition profiles in the grain boundary vicinity with high precision. These results have been useful in identifying the involved reaction mechanisms and the particular role of grain boundaries in the precipitation processes.

Fig. 4 is an example of a lattice image of a grain boundary precipitate in an Al-9.5 at .%Zn alloy aged 30 mins. at 180°C. The boxed region in (a) is shown enlarged in (b), indicating the region from which compositional analysis is performed. Fringe spacings were measured within both matrix (M) and precipitate (P) areas, at increasing distances from the grain boundary. The results are presented in Fig. 5, each point indicating the average spacing of ten fringes, with a representative scatter band showing the limits of experimental error.

This plot clearly indicates a decreasing fringe spacing as the boundary (dotted line) is approached from either side. It suggests that a solute gradient exists within both the matrix and the precipitate, and the concentration changes rapidly over a distance of only 50Å. Confirmation of this suggestion awaits application of STEM microanalysis-a capability now being installed on our EM 301 microscope. However one feature revealed by the lattice image method is that the segregation appears to be orientation dependent. Thus the power of combining different techniques is apparent.

C. Spinodal Decomposition, (C. K. Wu)

We have had considerable interest in characterizing the morphology of spinodal decomposition by conventional and more recently, high resolution techniques[8,9]. The latter method using lattice fringe imaging and optical microdiffraction has proven to be extremely useful in analyses of the early stages of the reaction, particularly since the composition variations are very small, and can easily escape detection by familiar imaging or spectroscopic techniques. Thus the variation of lattice parameters with spinodal wavelength down to ~10Å can be determined in this way[9].

Another application of the lattice imaging method has been the distinction between modes of decomposition in the critical vicinity of the coherent spinodal which is inside the chemical spinodal but which is not known for the Au - Ni system. Figure 6 shows an example for alloys aged near the vicinity of what is expected to be the coherent spinodal. The lattice image (a) clearly distinguishes the "typical" zone segregation whilst, (b) has the sinusoidal periodicity typical of spinodals. A significant result of this research is that the decomposition appears to be one dimensional in the early stages.

3. Refractory Ceramics - Silicon Nitride and Sialons

A. Intergranular Phases, (D. Krivanek, T. M. Shaw)

The potential advantages of refractory ceramics for high temperature applications e.g., gas turbines and liquid metal containers are well recognized since they have very attractive properties (high modulus: density ratios, high melting points, oxidation resistance, etc.). However, due to fabrication difficulties the use of hot-pressing additives such as MgO or Y_2O_3 are needed and the properties at high temperatures are impaired. It has been proposed that the impairment is due to the formation of an intergranular phase, probably glassy as a result of the formation of silicates and crystalline oxy nitrides. Attempts to prove this have been successful using high resolution TEM[10,11]. The problem of resolving intergranular phases and whether they are amorphous or not is however not trivial. From an electron microscopy viewpoint therefore, the following features at grain boundaries require characterization: 1) detecting

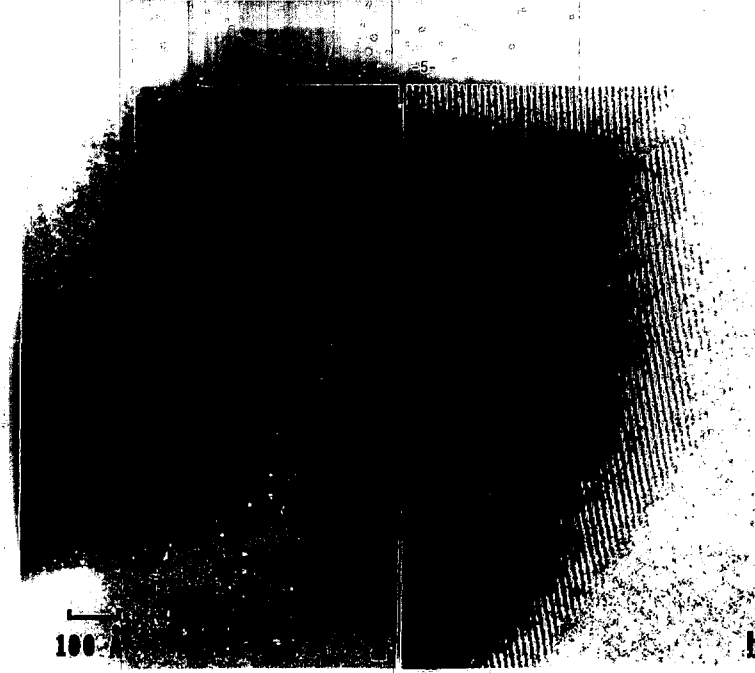

XBB 7611 10514A

FIG. 4(a)

XBB 7611 10514A

FIG. 4(b)

FIG. 4

(a) Lattice image of a grain boundary precipitate in an Al-9.5 at.%Zn alloy.

(b) Enlargement of boxed region in (a); Matrix image of (111); precipitate (0002 fringes).

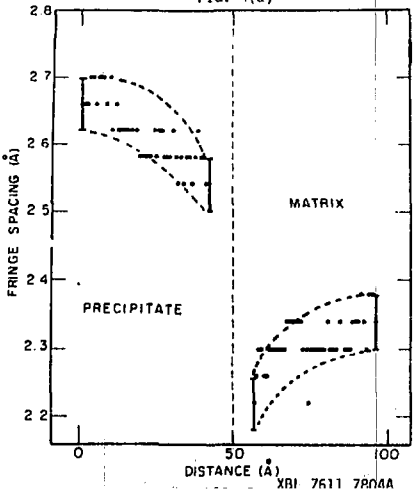

XBL 7611 7804A

FIG. 5

Plot of fringe spacing as a function of distance from the grain boundary in Fig. 4 (dotted lines). Each point represents 10 measurements. The data clearly show a gradient in lattice parameter and hence composition.

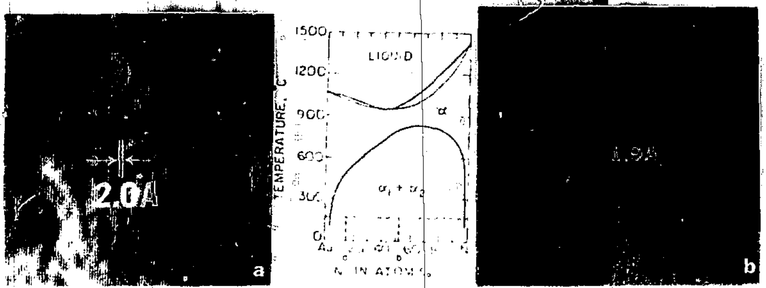

XBB 7711 11454
FIG. 6(a)

XBB 7711 11454
FIG. 6(b)

[illegible] of 200 planes in Au-Ni alloys [illegible] typical [illegible] Zones and alloy [illegible] the coherent [illegible] diagram in center.

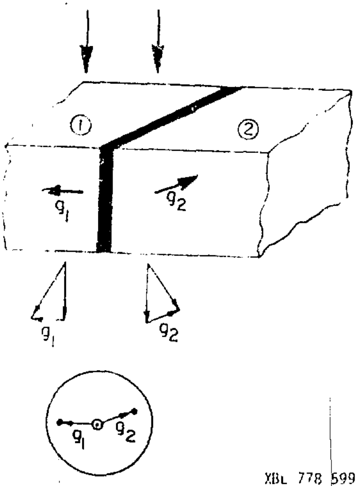

XBL 778 5991

FIG. 7

the intergranular phases and their distribution, 2) determining whether the [illegible] are crystalline, and 3) determining their chemical compositions.

From a morphological viewpoint it is essential to choose the proper [illegible] conditions as sketched in Fig. 7. Under conventional imaging [illegible] the grain boundary should be viewed edge-on with simultaneous strong [illegible] grains. The contrast from intergranular phases if present and [illegible] whether they are amorphous or crystalline. Amorphous phases [illegible] generally appear in light contrast [illegible] Figs. [illegible](a) and 9(b). Dark field [illegible] preferable to enhance grain boundary [illegible] ionisation radiation damage [illegible] exposure to the electron beam [illegible] it becomes apparent which [illegible] and 8(b). [illegible] diffraction pattern. Dark field [illegible] in Fig. [illegible] [illegible] very narrow intergranular [illegible] glassy phases. [illegible] [illegible] with enough [illegible]

[illegible] field lattice imaging technique [illegible] grain boundary [illegible] a perfect edge [illegible]

[illegible]

[illegible] very wide grain boundaries [illegible] grain boundary [illegible] detectability [illegible] materials [illegible] considerably superior high-temperature [illegible]

[illegible] light elements [illegible] elements for [illegible] [illegible] Fig. [illegible]

Magnetic Materials: Garnets, [illegible]

[illegible] Gallium Germanium Garnet (GGG) can be used as [illegible] material for [illegible] devices. In such applications a thin magnetic [illegible] grown [illegible] on the substrate. Consequently, defect free substrate single crystals are desired since inhomogeneities in the substrate can be replicated in the epitaxial film and lead to degradation of device performance.

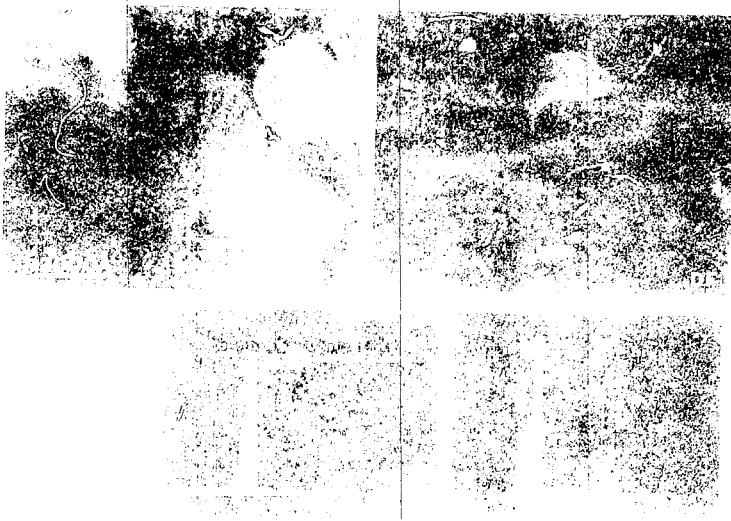

12. G. M. Jenkins, K. Kawamura, and L. L. Ban, Proc. Roy. Soc. (Lond) A327, 501-517 (1972).

13. V. A. Phillips, Metallography 6, 361-364 (1973).

14. S. Boyer, U. Dahmen, R. H. Bragg and G. Thomas, J. Amer. Ceram. Soc., 61, 174 (1978).

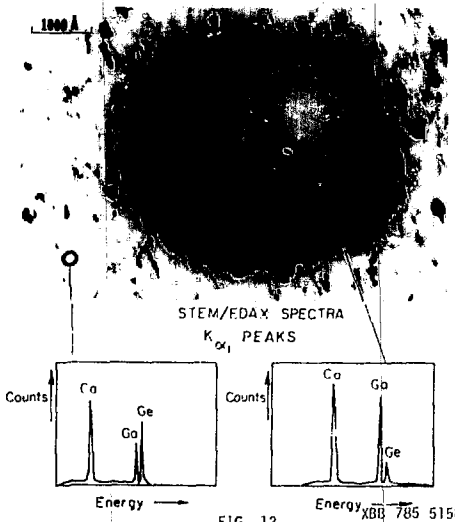

FIG. 12

FIG. 12

650 kV Bright field high order image showing microsegregation defect. Stereoanalysis showed that this is a spherical defect (hole or gas-filled cavity), surrounded by dark contrast. A 200A probe was placed in each of the areas shown. The EDAX spectra obtained shows the defective region to be rich in Co and Ge and depleted in Ge relative to the matrix material. Thus the defects occur due to microsegregation of elements intrinsic to the CGGG system. (Specimen courtesy of Phillips, Eindhoven).

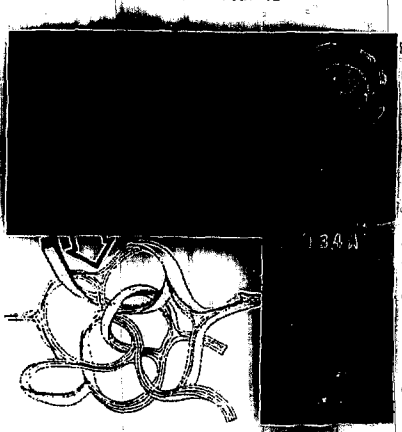

FIG. 13

FIG. 13

Lattice image of glassy carbon showing isotropic distribution of interwoven fibers. The imaging condition is shown in the inset SAD. Note the spotty appearance of the 002 ring when a very small area is selected for diffraction.

The fibers are crystalline and tend to enclose very small pores at points of bifurcation (arrows), confirming Jenkins' "nightmare" model of glassy carbon (see sketch) and results obtained from small angle X-ray scattering.